1

McClay, Ken, 2011, Introduction to thrust fault-related folding, *in* K. McClay, J. H. Shaw, and J. Suppe, eds., Thrust fault-related folding: AAPG Memoir 94, p. 1–19.

Introduction to Thrust Fault-related Folding

Ken McClay

Fault Dynamics Research Group, Department of Earth Sciences, Royal Holloway University of London, Egham, Surrey, United Kingdom

ABSTRACT

The 16 chapters presented in this memoir cover some of the recent advances made in the descriptions and analysis of thrust-related fold systems. The chapters include kinematic and geometric analyses of fault-propagation folding, trishear folding, detachment folding, wedge-thrust fold systems, and basement-involved thrust systems. Examples are given from the Zagros fold belt of Iran; the sub-Andean fold belt of western Argentina; the frontal fold belt of the Tianshan, northern margin of the Tarim Basin in western China; from the fold and thrust belts of the Spanish Pyrenees, Taiwan, Wyoming, and southern California; as well as the deep-water fold belts of offshore Brazil and the Niger Delta. In particular, several chapters focus on new analyses of detachment folding as well as improved kinematic and geometric models of thrust-related folding. Improved seismic imaging combined with theoretical, numerical, and analog modeling, plus the detailed field studies as presented in this volume, indicates the range of challenges and the strategies that can be brought to bear in integrating the well-established geometric and kinematic models of thrust fault-related folding with mechanical models to account for the natural complexities of real-world structures. I hope that the readers of this memoir will find these new ideas and concepts relevant for the exploration and exploitation of hydrocarbon systems in fold and thrust belts worldwide.

INTRODUCTION

Thrust fault-related folds form hydrocarbon traps in many fold and thrust belts, from subaerial fold belts such as the Zagros of Iran and Iraq (e.g., Beydoun et al., 1992; Sherkati et al., 2006; Cooper, 2007), and the sub-Andean fold and thrust belt of South America (Figure 1a) (Echavarria et al., 2003; also see Tankard et al., 1995), to deep-water fold belts such as offshore northwest Borneo (e.g., James, 1984; Sandal, 1996) (Figure 1b) and offshore west Africa in the Niger Delta (e.g., Figure 1c) (Ajakaiye and Bally, 2002; Bilotti and Shaw, 2005; Corredor et al., 2005a, b).

Understanding and recognizing the two-dimensional (2-D) and three-dimensional (3-D) geometries of thrust fault-related fold structures and how hanging-wall folds develop are vital for the exploration and exploitation of hydrocarbons in both subaerial and submarine fold belts. In particular, the geometric and kinematic models of thrust-related folding have been instrumental in guiding the interpretation of structural styles of thrust belts in the subsurface (e.g., Suppe, 1983, 1985; Suppe et al., 1992, 2004; Shaw et al., 2005) and for the construction of balanced cross sections (Guzofski et al., 2009). Many of these models have been incorporated into the algorithms used in computer programs for cross section

DOI:10.1306/13251330M9450

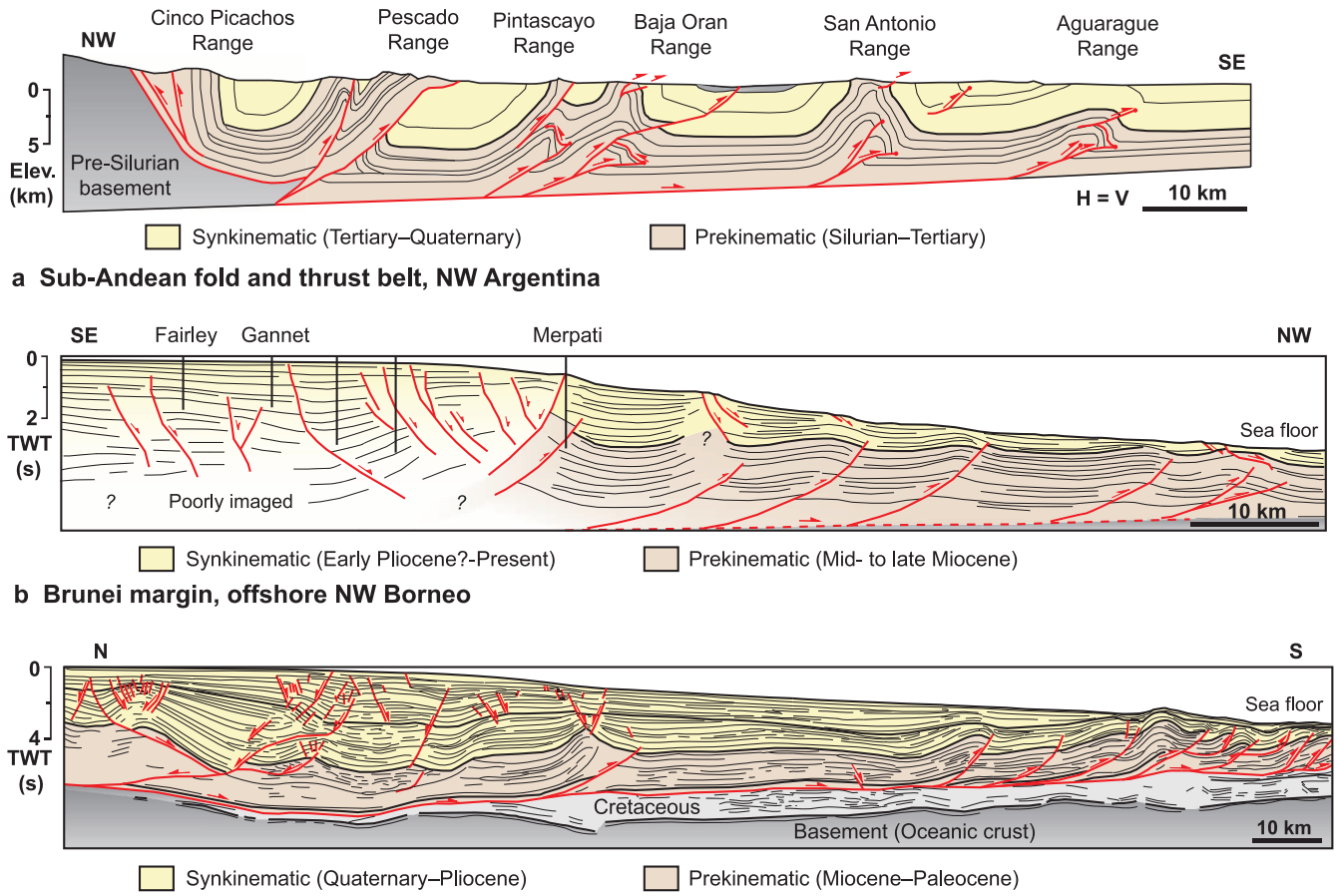

Figure 1. Fold-thrust structures in three hydrocarbon-bearing fold and thrust belts. TWT (s) = two-way traveltime in seconds; H = V; horizontal = vertical scales; Elev. = elevation. (a) The sub-Andean fold and thrust belt of northwestern Argentina. Significant hydrocarbon accumulations have been found in the complex fault-related fold systems in the frontal sectors of the belt (modified from Echavarria et al., 2003). (b) Schematic section through the near-shore to deep-water offshore Brunei margin, northwest Borneo. Thrust-related folds are developed in the slope and toe section of the Barram delta complex due to regional contraction (modified from Sandal, 1996). (c) The eastern lobe of the Niger Delta, Gulf of Guinea, showing gravity-driven contraction and the development of thrust fault-related folds at the delta toe region (modified from Ajakaiye and Bally, 2002).

construction, for retrodeforming and balancing cross sections, as well as for predictive forward modeling of strain and fracture distributions within hydrocarbon reservoirs in thrust-related fold structures.

Since the benchmark articles of Suppe (1983, 1985) and coworkers (Suppe and Medwedeff, 1990) on predictive geometric models of thrust-related, fault-bend folds and fault-propagation folds, considerable research and many publications have focused on evaluating, refining, and applying these models to thrust terranes in both two and three dimensions (e.g., Suppe, 1983; Suppe and Medwedeff, 1990; Erslev, 1991, 1993; Jordan and Noack, 1992; Suppe et al., 1992, 2004; Narr and Suppe, 1994; Epard and Groshong, 1995; Homza and Wallace, 1995; Poblet and McClay, 1996; Erslev and Mayborn, 1997; Hardy and Ford, 1997; Medwedeff and Suppe, 1997; Poblet et al., 1997; Storti and Poblet, 1997; Allmendinger, 1998; Zehnder and Allmendinger, 2000; Atkinson and Wallace, 2003; Mitra, 2003; Gonzalez-Mieres and Suppe, 2006; Hardy and Connors, 2006).

The inclusion of synkinematic growth strata into these kinematic models of thrust-related folding (e.g., the benchmark article of Suppe et al., 1992) was a major step forward and focused the attention on the possibilities of extracting quantitative information from thrust-related fold systems both in subaerial and submarine environments (e.g., Hardy et al., 1996, Poblet et al., 1997; Storti and Poblet, 1997; Suppe et al., 1997, 2004; Allmendinger, 1998; Shaw et al., 2005; Gonzalez-Mieres and Suppe, 2006). The different kinematic models for these thrust-related folds give different predictions for the rates and distributions of instantaneous uplift of

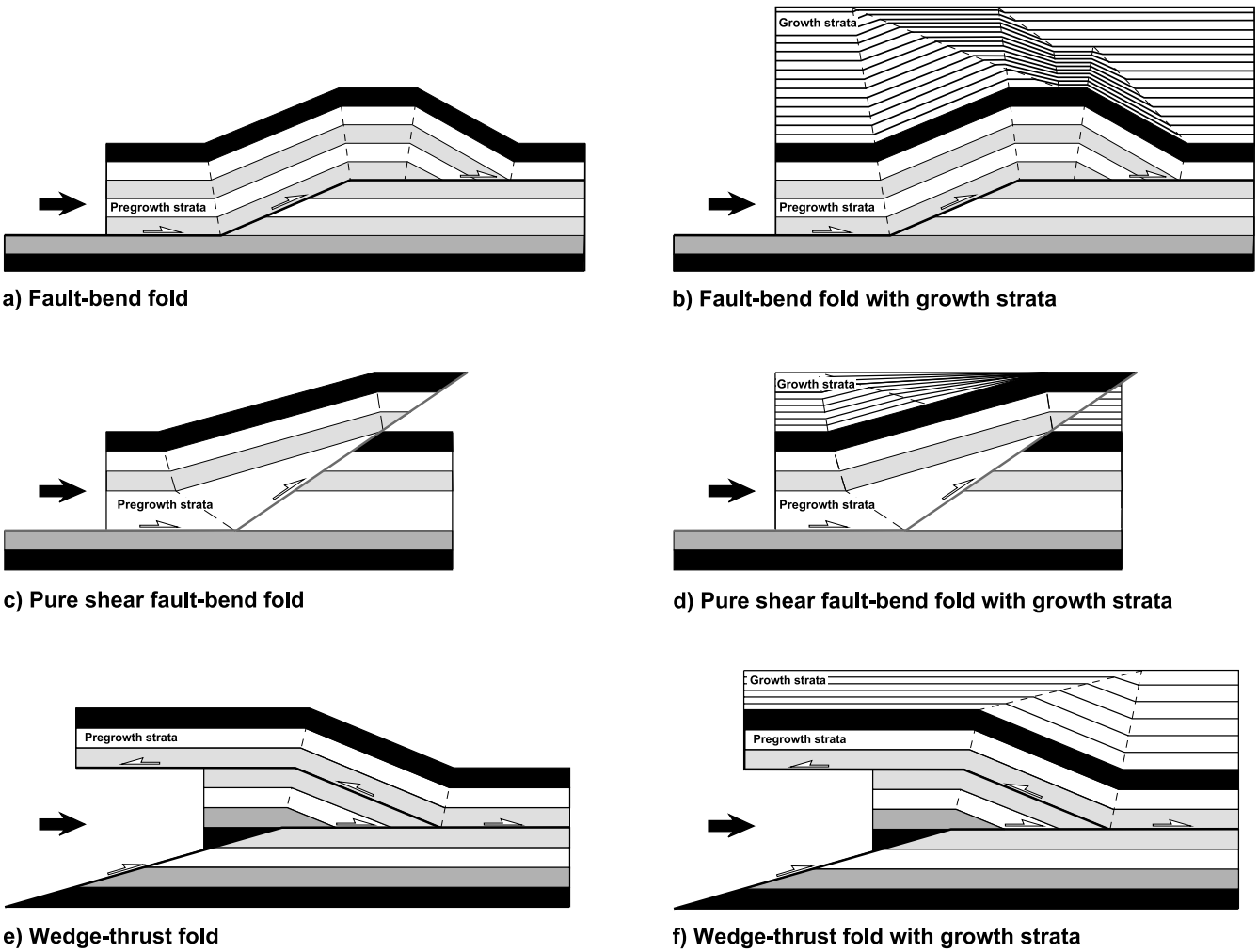

Figure 2. Thrust-related fault-bend folds with and without synkinematic growth strata. (a) Kink-band fault-bend fold (modified from Suppe, 1983). (b) Kink-band fault-bend fold with growth strata (modified from Suppe et al., 1992). (c) Kink-band, pure shear fault-bend fold (modified from Suppe et al., 2004). (d) Kink-band, pure shear fault-bend fold with growth strata (modified from Suppe et al., 2004). (e) Wedge-thrust fold system (modified from Medwedeff, 1989; Shaw et al., 2005). (f) Wedge-thrust fold system with growth strata (modified from Medwedeff, 1989; Shaw et al., 2005).

the fold crest relative to total fold uplift. The resultant growth stratal patterns in general will be different for each of these various kinematic models and therefore may be used to infer the style of fault-related folding and also to quantify fault slip and fold uplift rates in detail (e.g., Hardy et al., 1996; Rivero and Shaw, 2011; Yue et al., 2011).

In 2005, the AAPG benchmark publication on seismic interpretation in contractional settings by Shaw et al. (2005) captured many of the recent advances in applying these geometric models to guide seismic interpretation and analysis of contraction-related fold structures. This current memoir presents further advances in the understanding of thrust fault-related folds, particularly applying other techniques such as numerical and physical modeling as well as documenting different fold styles in a variety of contractional regimes, from delta toe-thrust belts to subaerial fold-belt systems. New theoretical as well as practical analyses of detachment fold systems are presented. New techniques are presented for the interpretation, analysis, and understanding of detachment folds that are common in deep-water fold belts as well as in subaerial fold belts.

This memoir includes chapters that analyze fault-propagation folding, detachment folding, wedge-thrust systems, basement-involved thrust systems, basin-inversion-related thrusting and folding as well as deep-water fold belts. Examples are given from the Zagros fold belt of Iran; the Spanish Pyrenees; the southern

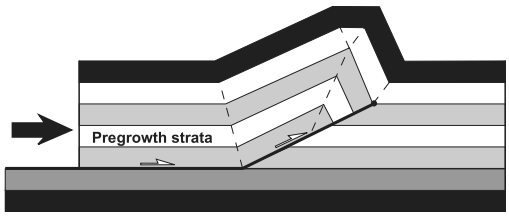

a) Fault-propagation fold

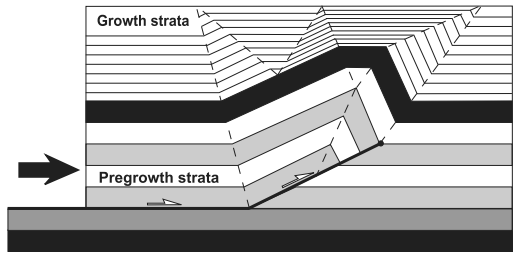

b) Fault-propagation fold with growth strata

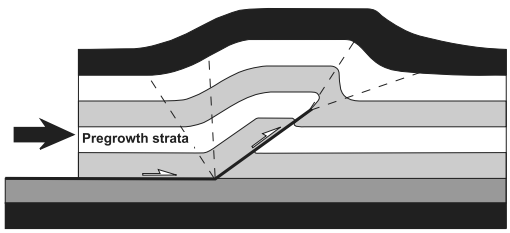

c) Trishear fault-propagation fold

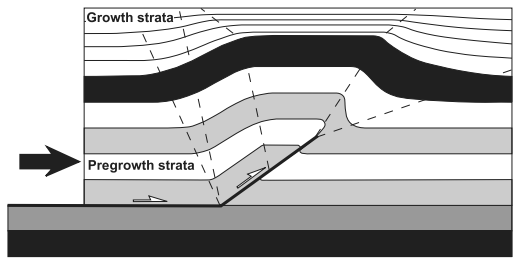

d) Trishear fault-propagation fold with growth strata

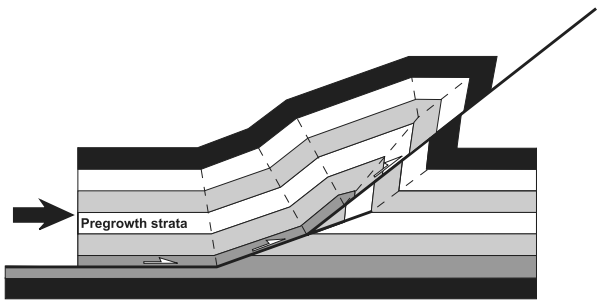

e) High-angle forelimb break-thrust fault-propagation fold

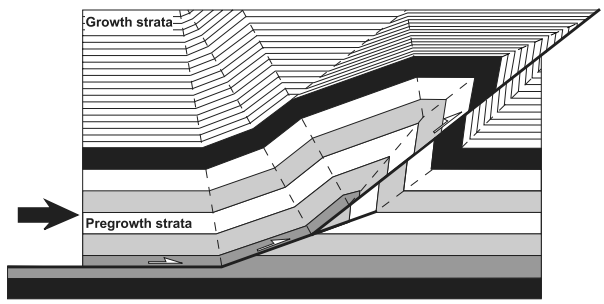

f) High-angle forelimb break-thrust fault-propagation fold with growth strata

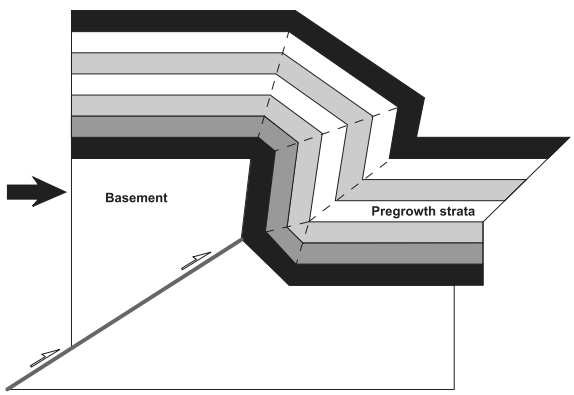

g) Basement-involved fault-propagation fold

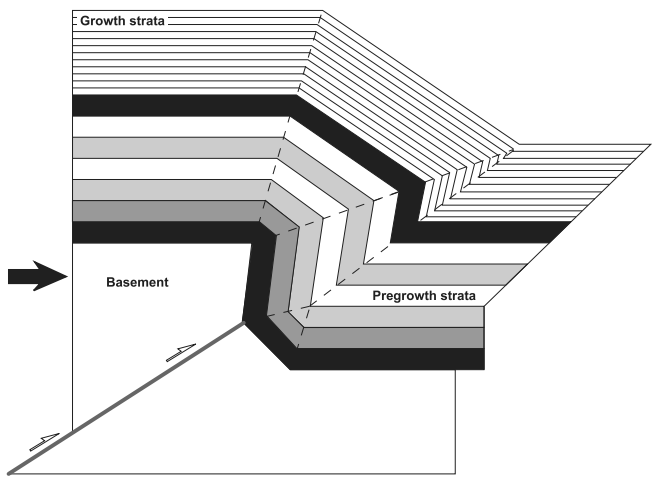

h) Basement-involved fault-propagation fold with growth strata

Tianshan fold and thrust belt of western China; and fold and thrust belts in Taiwan, Argentina, Wyoming, offshore California as well as offshore Brazil and the offshore Niger delta.

THRUST-RELATED FOLD SYSTEMS

In this part of the introductory chapter, the principal types of kink-band, thrust-related fold systems are briefly reviewed and their key geometric characteristics are highlighted. Figure 2 summarizes the finite deformed state geometries of many of the kinematic models for fault-bend fold-type structures that have been published in the past two decades, whereas Figure 3 shows examples of fault-propagation fold systems. Figure 4 summarizes some of the key elements of detachment fold systems. Examples of these thrust-related fold geometries are given in Figures 5–10.

In these kink-band-style models, the dominant deformation mechanism is assumed to be bed-parallel slip between the layers (e.g., Suppe, 1983, 1985; Suppe and Medwedeff, 1990; Suppe et al., 1992, 1997; Shaw et al., 2005). In general, the layer thickness is constant except in some detachment fold models where the ductile flow of material into and out of the fold core may be required (cf. Poblet and McClay, 1996).

Many of these geometric fold models are self-similar in that, as the fold amplifies, the limb dips remain constant and the limb lengths change by kink-band migration (Suppe, 1983; Suppe et al., 1992). In these self-similar models, fold amplification does not change the fundamental geometric architecture of the fold through time. In contrast, geometric models of folds where the limb dip changes as the fold amplifies are termed ''non-self-similar'' whereby the fold geometry changes through time mostly by progressive or episodic limb rotation (Hardy and Poblet, 1994; Poblet and McClay, 1996; Poblet et al., 2004). These progressive changes in limb dip result in fanning growth strata on both the front limbs and backlimbs as the fold amplifies (e.g., Figure 4b, c) (Poblet et al., 1997).

Seismic examples of thrust fault-related folds are shown in Figure 5, and outcrop examples are shown in Figure 6. Comparative natural examples of growth stratal geometries are shown in Figure 7. Scaled physical modeling (e.g., Wu and McClay, 2011) and numerical modeling (Hardy and Allmendinger, 2011) have been extensively used to simulate thrust-related fold systems, and typical examples are shown in Figures 8 and 9.

Fault-bend Folds

Fault-bend folds are generated above steps in the underlying thrust fault-producing folds in the hanging wall, whereas the footwall section remains undeformed (Figure 2). Suppe (1983) published a benchmark article on the geometric analysis of kink-band-style fault-bend folds demonstrating the key relationships between ramp geometries and the overlying hanging-wall anticline and syncline folds (e.g., Figure 2a). In these kink-band models of fault-bend folding, the thrust fault has propagated across the entire section, and subsequent displacement of the hanging wall over this stepped fault trajectory produces kink-band folds with constant limb dips. Amplification of the fold occurs through kink-band migration as the hanging wall is translated over the stepped footwall thrust surface (Figure 2a). Deformation within the fold is accomplished by flexural slip between the layered units. Fold axial surfaces bisect the interlimb angles between different dip domains of the fold limbs.

In 1992, Suppe et al. added growth sequences to these fault-bend fold models (Figure 2b) and demonstrated how quantitative analyses of these synkinematic units could be used to determine fold uplift and shortening rates. Suppe et al. (2004) further modified the theory of kink-band fault-bend folding to include folds where the thrust fault trajectory cuts across the layers with resultant internal shearing and named these ''shear fault-bend folds'' (Figure 2c). This kinematic model of shear fault-bend folding accounts for the geometries of fault-bend folds where the hanging-wall strata dip at lower angles than the underlying thrust ramp as well as for fanning growth strata on the back limbs of such folds (e.g., Figures 2d, 5a).

Shaw et al. (2005) discussed the various geometries of kink-band folds produced by wedge thrusts where an allochthonous section is thrust into an undeformed section with an overlying back thrust (Figure 2d, e). Wedge thrusts are commonly developed at the frontal sections and terminations of fold and thrust belts in highly anisotropic strata such as in the deep-water turbidites at the front of the Mahakam delta (Figure 5b).

Figure 3. Fault-propagation folds with and without synkinematic growth stratal architectures. (a) Fault-propagation fold; (b) fault-propagation fold with growth strata; (c) fore- and backlimb trishear fault-propagation fold; (d) trishear fault-propagation fold with growth strata; (e) high-angle forelimb break-thrust fault-propagation fold; (f) high-angle forelimb break-thrust fault-propagation fold with growth strata; (g) basement-involved fault-propagation fold; (h) basement-involved fault-propagation fold with growth strata (modified from Suppe et al., 1992, 2004; Narr and Suppe, 1994; Poblet et al., 1997; Shaw et al., 2005).

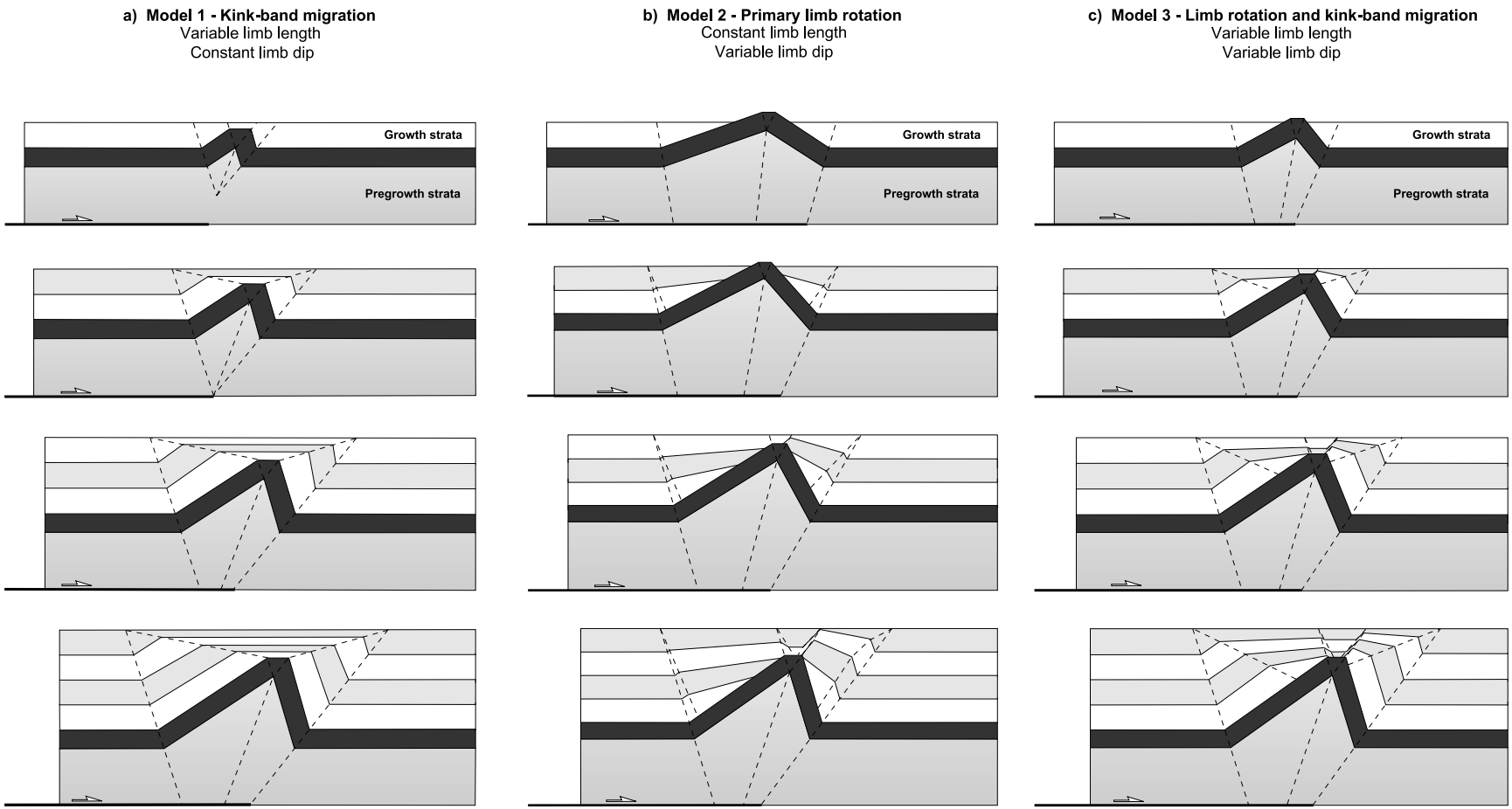

Figure 4. Detachment fold systems. Three modes of detachment fold growth as described by Poblet and McClay (1996) and Poblet et al. (1997). All three models show the progressive evolution of detachment growth folds with successive, equal increments of shortening at high synkinematic sedimentation rates: (a) model 1, deformation by kink-band migration and variable limb length; (b) model 2, deformation by progressive limb rotation and constant limb length; (c) model 3, combination of limb rotation and variable limb length.

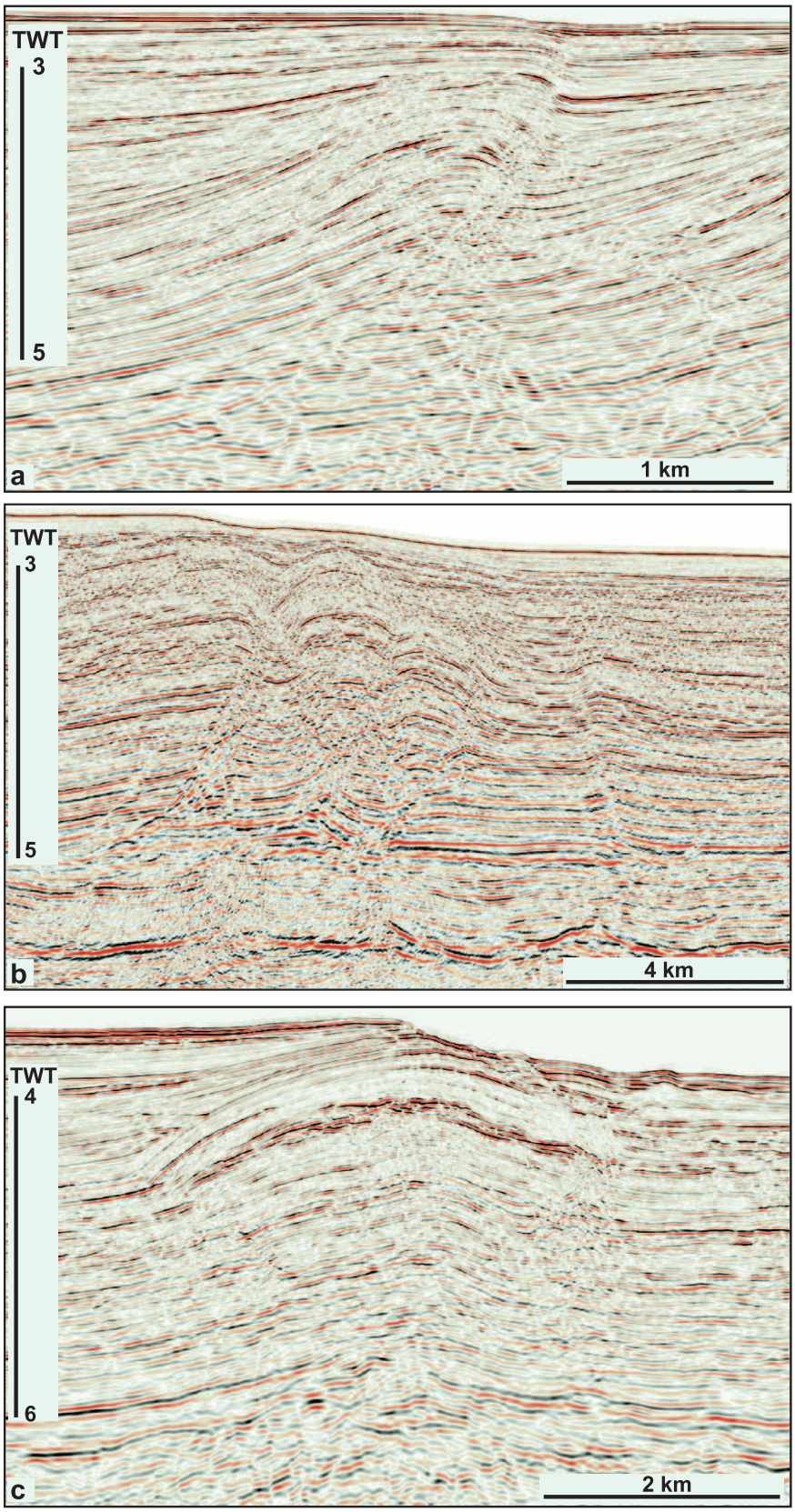

Figure 5. Seismic examples of thrust-related fold systems. Vertical scales are two-way traveltime (TWT) in seconds. (a) Fault-propagation fold, deep-water Niger Delta (seismic data courtesy of CGGVeritas). (b) Fault-propagation folds and wedge thrust folds, Mahakam fold belt, Makassar Straits, Indonesia (seismic data courtesy of TGS Nopec). (c) Detachment fold, deep-water Niger Delta (seismic data courtesy of CGGVeritas).

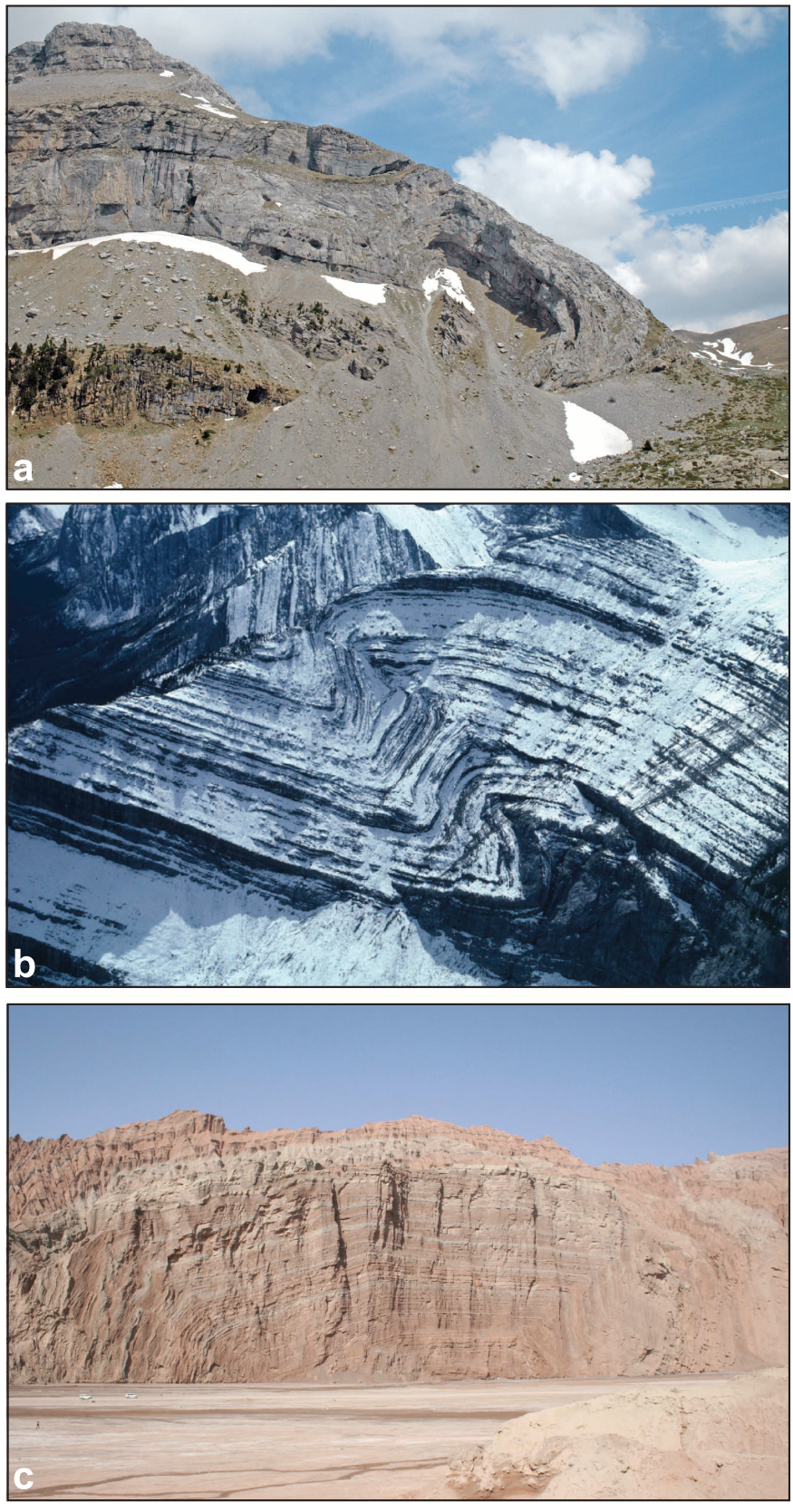

Figure 6. Outcrop examples of thrust-related fold systems. (a) Transported fault-propagation fold, Puerto de Aragues, Spanish Pyrenees. The hanging-wall section consists of Upper Cretaceous sandstones (brown) and overlying, folded Paleocene limestones (gray) thrust over a footwall section of Paleocene limestones. Field of view is approximately 300 m (984 ft). (b) Asymmetric detachment fold in the Mississippian Mount Head limestones, southern Canadian Rocky Mountains. Field of view is approximately 450 m (1476 ft). (c) Box geometry detachment fold in Miocene mudstones and siltstones above an evaporitic detachment; Quilitak anticline, southern Tianshan, western China. Field of view is approximately 600 m (1969 ft). Note vehicles for scale in lower left of photo.

Fault-propagation Folds

Figure 3 summarizes some of the key, kink-band-style geometric models of thrust fault-propagation folding. Suppe (1985) and Suppe and Medwedeff (1990) formalized the kink-band geometric model for thrust fault-propagation folding where a hanging-wall anticline-syncline fold pair forms at the leading edge of the thrust fault. This fold pair is tied to the fault tip line, which is located on the ramp and climbs up stratigraphic section in the direction of tectonic transport with progressive fault displacement (Figure 3a). This fault-propagation fold model develops by kink-band migration such that the limb dips form instantaneously as the fold starts to develop and do not change as the fold amplifies (i.e., constant limb dip). Fault-propagation folds are very common in fold and thrust belts particularly where steep to overturned front limbs occur (e.g., Figures 5a, 7c, d). In the simplest kink-band model for a fault-propagation fold with a high rate of synkinematic sedimentation, characteristic growth triangles with inclined axial surfaces are developed (Figure 3b). These are significantly different from the growth geometries formed by simple fault-bend folds (Figure 2b) and may possibly be used to differentiate between these two models for thrust-fault-related folding.

Erslev (1991) introduced the concept of ''trishear'' fault-propagation folding whereby the front limb of a fault-propagation fold developed by progressive limb rotation with differential shear between two inclined axial surfaces (Figure 3c). In this model, the dips of the anticline front limb increased downward toward the fold tip line. The addition of growth strata and the development of models with triangular shear in the backlimb synclinal hinge region resulted in fault-propagation fold models where fanning growth strata were developed on both the front limbs and backlimbs (e.g., Figure 3d). Fault-propagation folds with fanning growth strata on both the front limb and backlimb are common in deep-water fold belts where syntectonic sedimentation rates are high and the structures are preserved (e.g., Figure 7c, d).

Transported (or translated) fault-propagation folds (Jamison, 1987; Shaw et al., 2005) are commonly developed where the anticline front limb becomes faulted and the previously formed fold is carried forward on the new fault (Figure 3e, f). This is termed a forelimb break thrust and the resultant fold geometry a hanging-wall transported fault-propagation fold (e.g., Figure 6a). In these transported fault-propagation folds, a small footwall syncline commonly remains underneath the break thrust (Figure 3e, f).

Basement-involved fault-propagation folds are formed where steep thrust or reverse faults in the basement propagate upward causing folding in the overlying strata (e.g., Figure 3g, h) (Narr and Suppe, 1994). These are commonly formed by inversion of preexisting extensional fault systems and generate complex basement uplifts such as those found in the Laramide uplifts of Wyoming or those in the Sierras Pampenas in western Argentina (Erslev, 1993).

Detachment Folds

It has been 100 yr since Buxtorf and others described the classic detachment folds formed in the Jura above the Triassic evaporites (cf. Buxtorf, 1907, 1916). Since then, various studies have described and discussed detachment folds in a variety of subaerial fold belts (Laubscher, 1965, 2008; Jamison, 1987), but it is only relatively recently that they have become more widely recognized in both subaerial fold belts and also in deep-water fold belts (e.g., Poblet and McClay, 1996; Poblet et al., 1997; Mitra, 2002, 2003; Shaw et al., 2005; Gonzalez-Mieres and Suppe, 2006).

Figure 4 summarizes the three principal detachment fold models discussed by Poblet and McClay (1996) together with the addition of high sedimentation rate and growth stratigraphy (Poblet et al., 1997). These detachment fold models are characterized by a competent upper layer, or lid, above a ductile decollement unit. It is generally assumed that during shortening, the ductile decollement unit initially flows into and subsequently out of the fold core as the fold amplifies and the section shortens.

These three simple models of detachment folds produce identical final fold geometries for the prekinematic competent layer but with different synkinematic growth stratal architectures (Figure 4) (Poblet et al., 1997). Model 1 (Figure 4a) has constant limb dip and amplifies by kink-band migration as shortening progresses. Model 2 (Figure 4b) has constant limb lengths and amplifies by progressive limb rotation, whereas model 3 involves both limb lengthening and limb rotation during fold amplification (Figure 4c).

The synkinematic stratal architectures associated with the three different kinematic models produce significantly different patterns that may be used to distinguish between the models. Models 2 and 3 show characteristic fanning growth stratal patterns associated with progressive limb rotation (Figure 4b, c). Note that these models may generate local synclines in the growth strata directly above the crest of the detachment anticline (Figure 4b, c).

Detailed studies of many fold and thrust belts, however, show that detachment fold systems may be much more complex than the simple models shown in Figure 4. Hybrid structures (cf. Marrett and Bentham, 1997; McClay, 2004) and transported thrust-related folds (cf. Jamison, 1987; Mitra, 2003; Shaw et al., 2005) have been

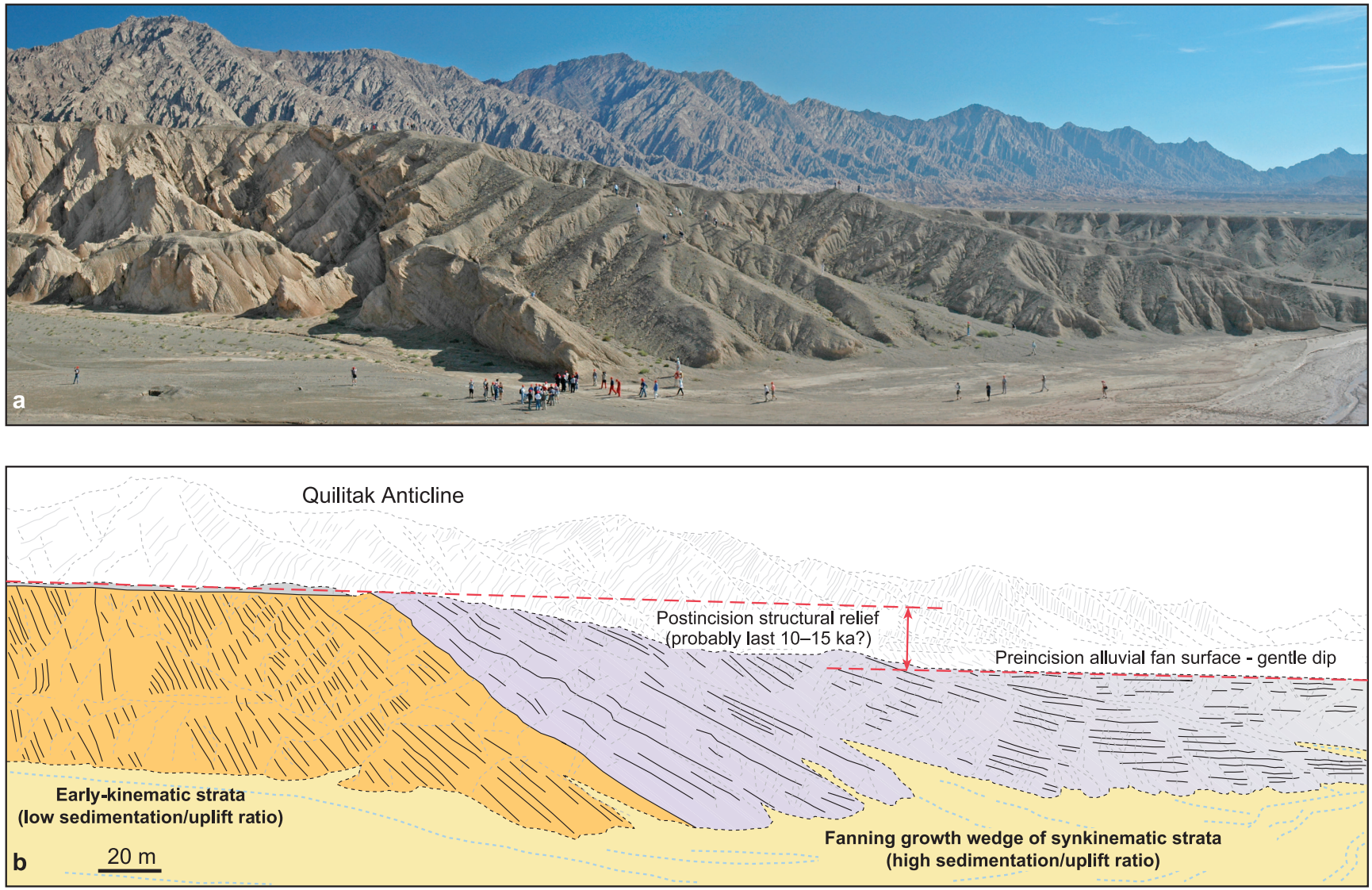

Figure 7. Examples of growth strata in fold and thrust belts. Vertical scales (c, d) are two-way traveltime (TWT) in seconds. (a) Alluvial fan growth wedges at the front of the Quilitak fold, Kuqa fold belt, frontal Tianshan ranges, western China. Light-colored early-kinematic gravels and sands (deposited at lower sedimentation rate relative to uplift rate) are overlain by successively younger, gray alluvial fan gravels and sands (deposited at higher sedimentation rate relative to uplift rate). The growth strata show fanning geometries with dips decreasing upward to the gently dipping preincision alluvial surface (after He et al., 2005; Hubert-Ferrari et al., 2007). (b) Interpretation of the growth wedge on the frontal limb of the Quilitak anticline showing light-colored early-kinematic gravels and sands overlain by an upwardly fanning wedge of Quaternary gray gravels and sands. The folding has been modeled by Hubert-Ferrari et al. (2007) as produced by progressive kink-band migration through an approximately 100-m (328-ft)-wide hinge zone.

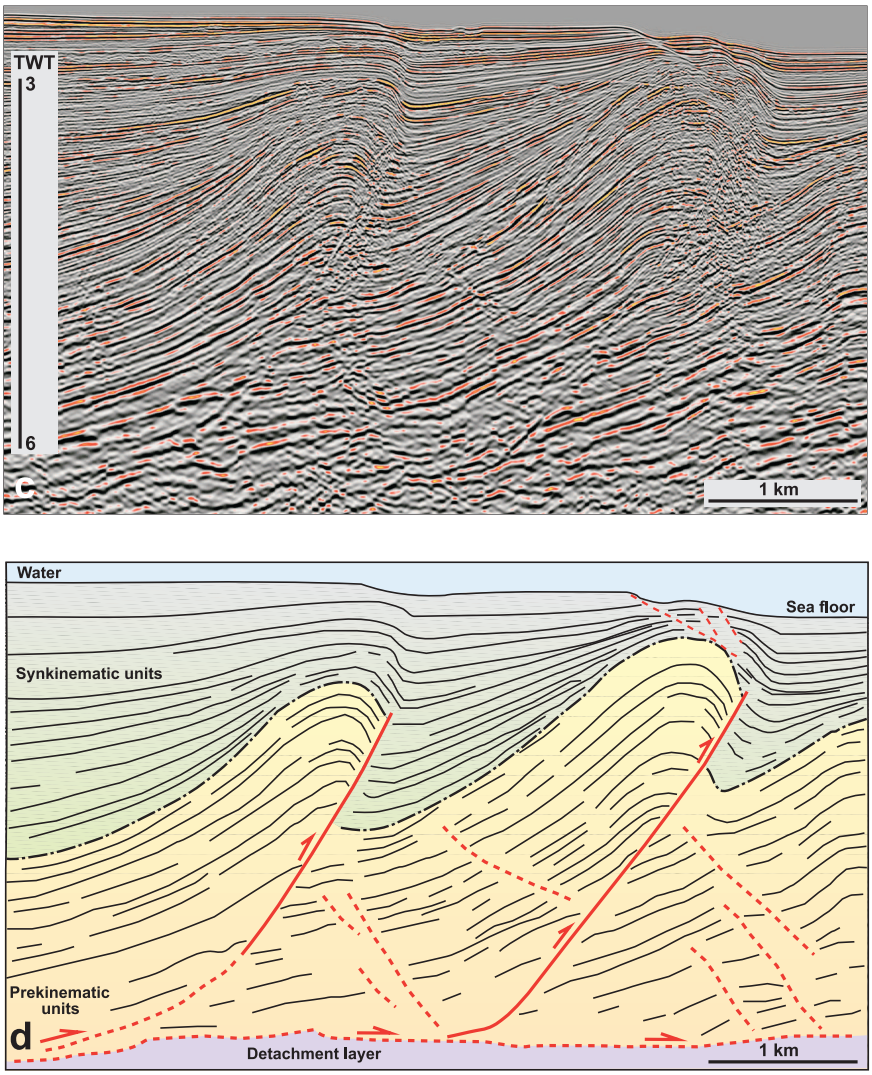

Figure 7. (cont.). (c) Seismic section through growth folds, frontal section of the toe-thrust fold belt, southwestern Niger Delta (seismic data courtesy of CGGVeritas). (d) Interpretation of the seismic section in panel c showing the synkinematic growth wedges on the front limbs and backlimbs of the fault-propagation folds.

recognized (Figure 10a). Mitra (2003) developed geometric and kinematic models for faulted symmetric and asymmetric detachment folds. Gonzalez-Mieres and Suppe (2006) analyzed low-amplitude detachment folds that grew by bed shortening and thickening, with almost no flexure, similar to the pure-shear detachment fold model of Groshong and Epard (1994).

Faulted detachment folds are characteristic in subaerial fold belts developed above salt detachments such as in the Zagros (see Mitra, 2003; McQuarrie, 2004; Sherkati et al., 2006; Vergés et al., 2011) and in deepwater fold and thrust belts where fold limbs are cut by low displacement thrusts (Figure 5c) (Shaw et al., 2005). Figure 10a shows a boxlike detachment fold where one limb has been cut by a thrust such that an asymmetric transported detachment fold has been developed. Note also the smaller back thrust that has displaced the backlimb producing a complex roof thrust system similar to the systems originally described by Buxtorf (1916) in the Jura and analyzed by Suppe (2011).

Outcrop examples of detachment folds in interbedded shales and sandstones commonly show complex imbrication and folding in their cores (Figure 10b, c). Numerical models of detachment folds in strata formed by alternating competent and incompetent units (such as turbiditic sandstones and shales) develop outer-arc extensional fault systems around the anticlinal hinges and smaller scale folds and out-of-syncline thrusts in the synclinal cores (Figure 9a). Similar structural styles are also formed in analog models of detachment folds (Figure 8c). These complexities in the cores of detachment folds are commonly poorly imaged on seismic sections such as those in the Niger Delta (Figure 5c).

In this memoir, descriptions and detailed analyses of various types of thrust fault-related folds are presented, and these chapters are briefly introduced below.

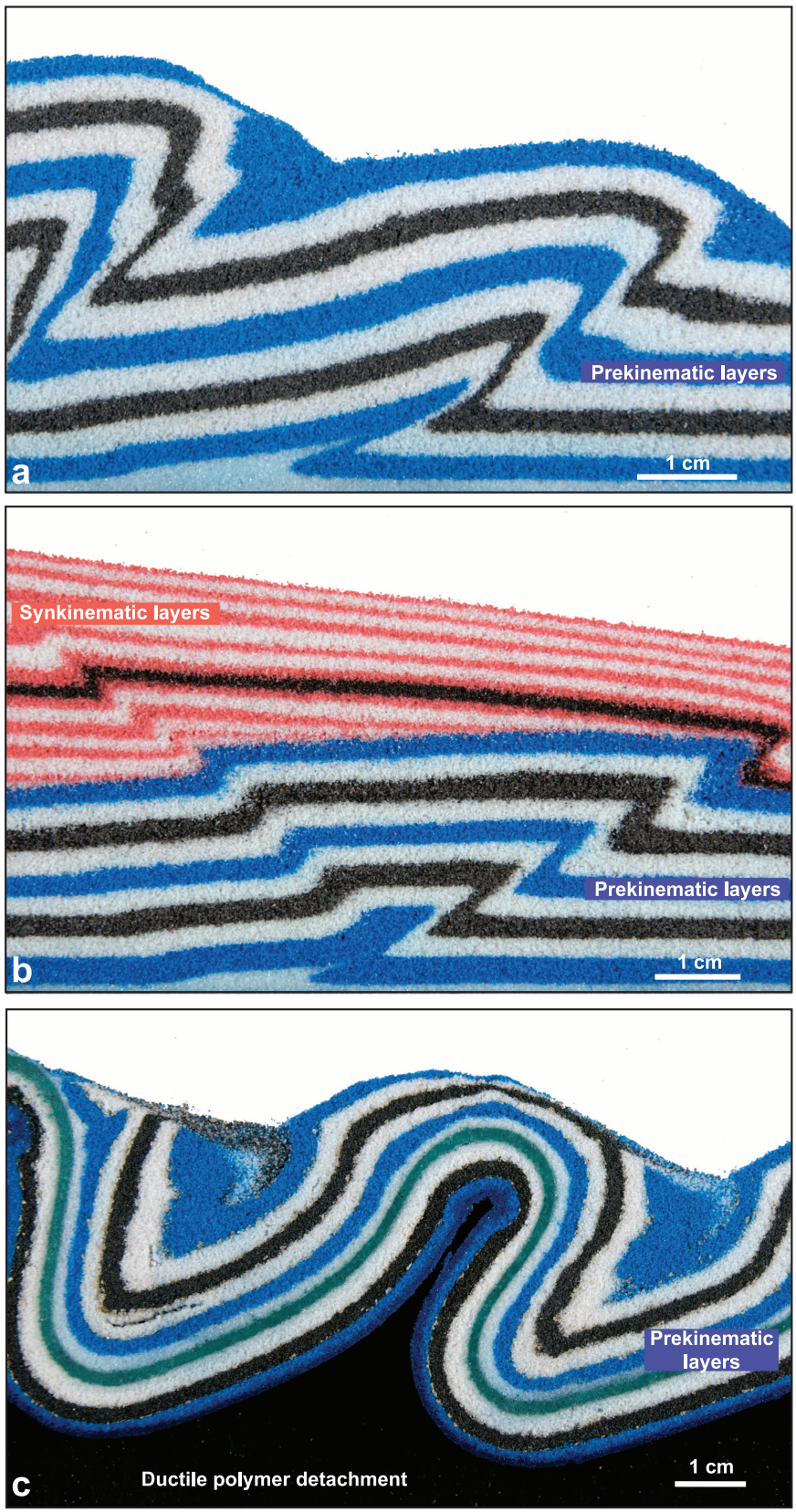

Figure 8. Scaled analog model examples of thrust-related fold systems. (a) Fault-propagation fold with rotated front limb and with the thrust ramp cutting across the hanging-wall strata. (b) Hybrid faulted detachment and fault-propagation fold with synkinematic growth strata onlapping the top limb of the hanging-wall box fold anticline. (c) Detachment folds showing lift-off geometries above a basal ductile polymer detachment layer. Ductile polymer has been squeezed out from the core of the anticline. Note also the small out-of-syncline thrusts in the core of the right syncline.

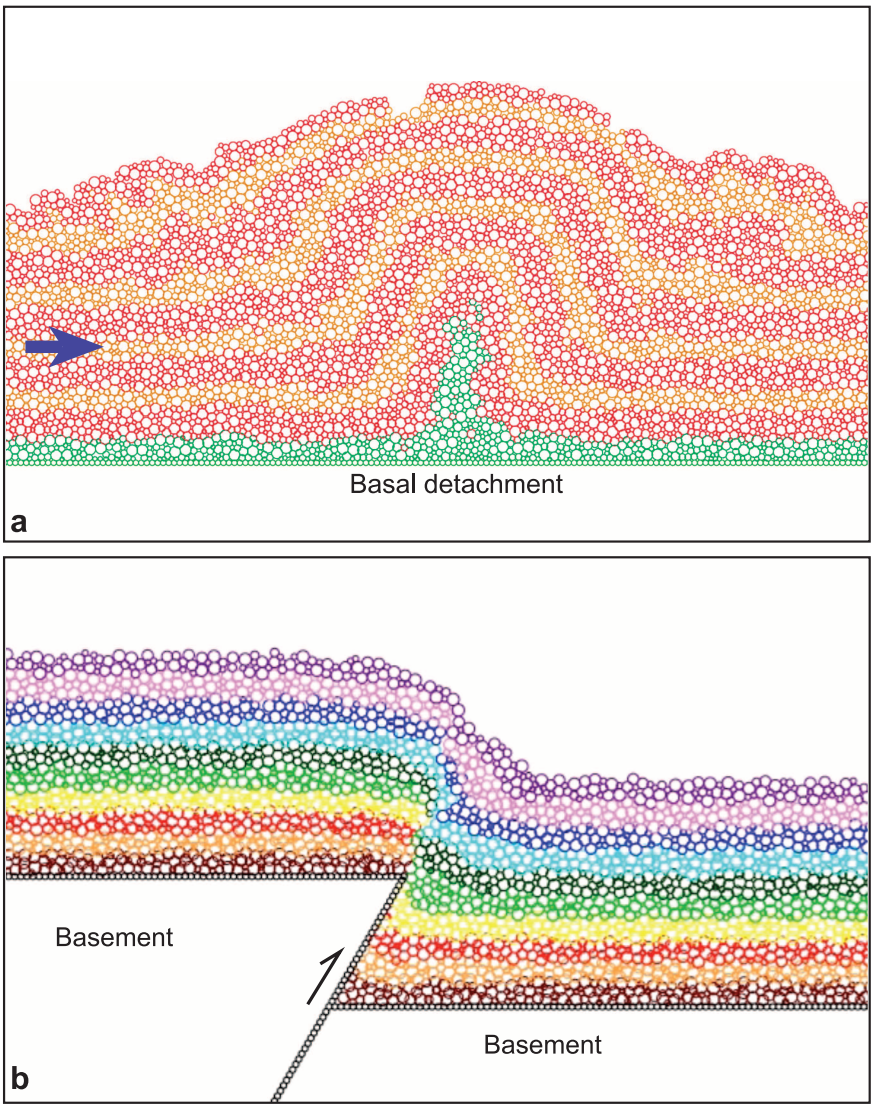

Figure 9. Distinct element numerical models (numerical sandbox) by Hardy and coworkers show how the mechanical stratigraphy and basement involvement control the fold geometries in the upper layers. Models are courtesy of Stuart Hardy (see also Hardy and Allmendinger, 2011). (a) Distinct element model of a detachment fold; (b) distinct element model of a basement-involved fault-propagation fold.

THIS VOLUME

The following sections introduce the 15 subsequent chapters in this memoir.

Thrust Fault-related Fold Models: Detachment Folds, Fault-propagation Folds, Shear Fault-bend Folds, and Wedge-thrust Systems

Chapter 2 by Suppe (2011) summarizes a new 2-D analysis of detachment folds, quantifying fold growth and evolution. The 2-D models of detachment folding analyzed in this chapter include classic ''closed systems'' where all of the strain is accommodated within the fold and ''open systems'' where out-of-the-plane flow of a weak ductile detachment layer accommodated the shortening or where a ''roof'' detachment or thrust occurs and accommodated shortening away from the principal fold. An early stage of pure shear folding is recognized before significant fold amplification and uplift develop. Examples from the classic cross sections of the Grechenberg railway tunnel in the Jura mountains drawn by Buxtorf (1916) are used to illustrate this new approach to understand detachment folds in thrust terranes.

Chapter 3 by Gonzales-Mieres and Suppe (2011) follows on from Chapter 2 by presenting new strategies for extracting detailed shortening histories of detachment folds based on area-of-relief measurements in growth strata, including the complexities of multiple detachments and flow of salt. These authors analyze active detachment folds in accretionary prisms such as the Nankai and Cascadia prisms as well as on the frontal fold system in the Kuqa fold belt, southern margin of the

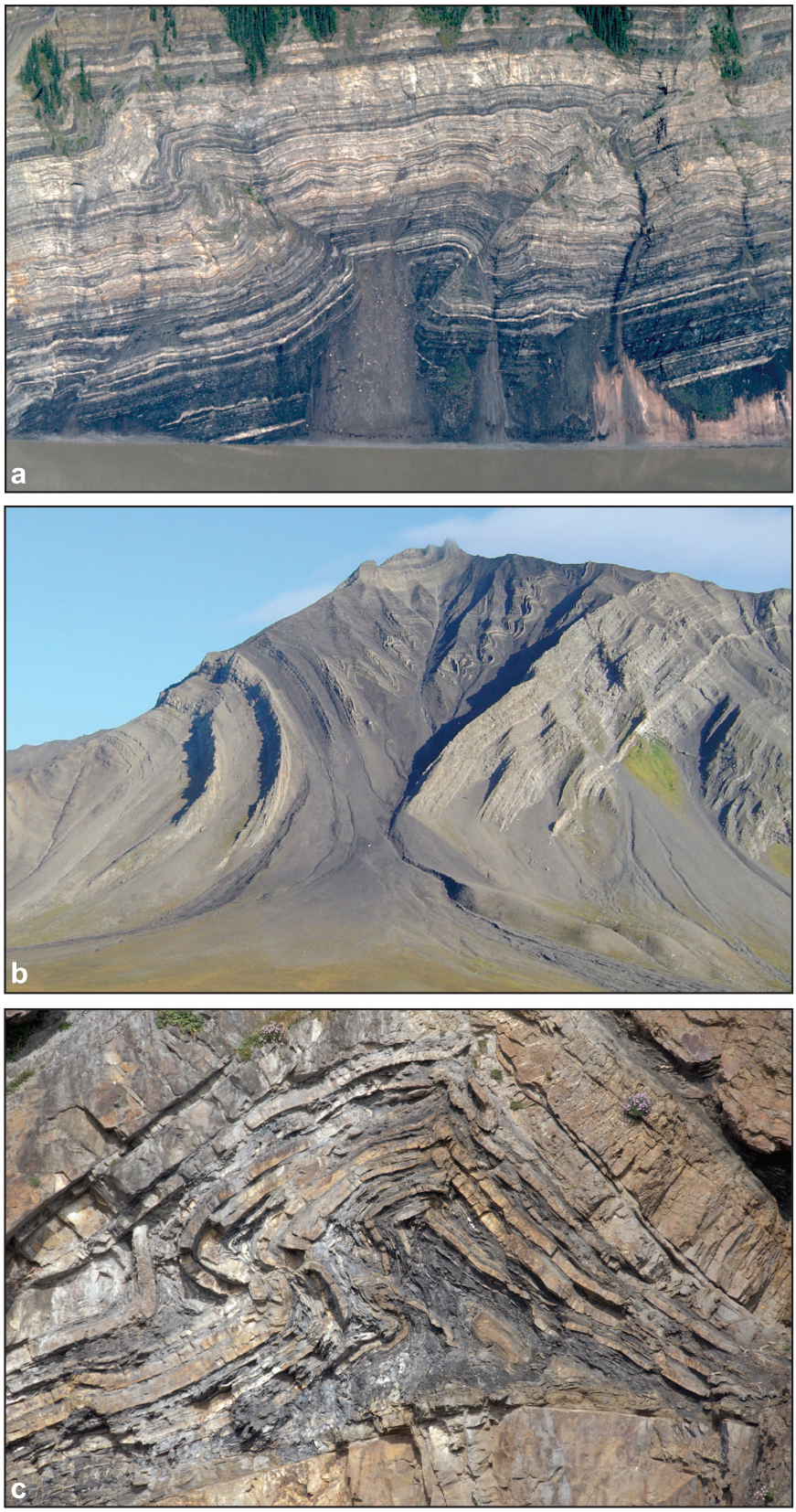

Figure 10. Detachment folds: examples of complex and hybrid structures. (a) Detachment fold with the front limb thrust in shale and limestone of the Pennsylvanian Calico Bluff Formation, Yukon River, Alaska. The cliff is approximately 250 m (820 ft) high (photo by Kevin Pogue, courtesy of Keck Geology Consortium). (b) Inclined boxlike detachment fold with inward-dipping limbs and internal folding accommodating space problems in the core of the anticline, Midterhuken peninsula, Spitsbergen (Maher et al., 1986). The units are Triassic shales and sandstones with the detachment surface sitting on top of the lower Bravaisberget formation sandstones, with intense chevron folding in black shales and thin siltstones above the detachment. The upper more competent "lid" is the sandy Upper Triassic De Geerdalen Formation. The height from the base of the photo to the uppermost peak is approximately 780 m (2559 ft) (photo courtesy of Alvar Braathen). (c) Detachment fold with thrusting and duplication in the core, North Cornwall. Note the complex accommodation structures around the hinge and core above the detachment surface. Units are Namurian age thick-bedded sandstones and interbedded shales. Field of view is approximately 5 m (16 ft).

Tianshan range, western China, and on the Agbami detachment fold, offshore Niger Delta. Episodic fold growth was documented in these examples with fault slip rates lower than the regional shortening rates.

Chapter 4 by Vergés et al. (2011) presents an elegant detailed description and analysis of the large Kabir Kuh fold structure in the southwest Zagros of Iran. This chapter focuses on the influences of multiple detachments and mechanical stratigraphy on the evolution of the fold system. This detailed analysis highlights the internal complexity of fold structures in what has previously been considered to be rather simple concentric-style folds in the simply folded belt of the southern Zagros (cf. Beydoun et al., 1992; McQuarrie, 2004; Sherkati et al., 2006).

Hardy and Allmendinger (2011) in Chapter 5 review the application of ''trishear'' kinematic models (cf. Erslev, 1991, 1993) to the study of fault-propagation folds with a focus on contractional tectonic settings. ''Trishear'' deformation has been used to develop models of progressive rotation of the front limbs of fault-propagation folds (Hardy and Ford, 1997; Allmendinger, 1998; Hardy and McClay, 1999) as well as forming fanning growth stratal wedges in these folds. The addition of backlimb trishear deformation in these kinematic models by Cristallini and Allmendinger (2002) has allowed the trishear model to be widely applied to fault-propagation growth folds where fanning growth strata are found on both the front limbs and backlimbs of a fault-propagation fold.

In Chapter 6, Tavani and Storti (2011) discuss the tip-line strain effects of the so-called ''double-edge fault-propagation folding'' model, a geometric variant of the model of faulting developing first within the competent layer and then propagating both up to the surface as well as down to the underlying detachment. This model may offer an alternative explanation to the ''shear fault-bend fold'' model (Suppe et al., 2004; Shaw et al., 2005) to explain fault-fold systems where the backlimb hanging-wall panel is not parallel to the fault at depth.

Alonso et al. (2011) in Chapter 7 describe a detailed analysis of folding mechanisms in a fault-propagation fold using key unconformities within the growth strata. This analysis shows how internal deformation may be distributed within an evolving fault-propagation fold with synkinematic growth strata. The results of this type of analysis are particularly important where growth strata are involved and where nonparallel layers of the synkinematic sequence are folded during uplift and amplification. In some circumstances, this may produce synclines in the growth sequence directly on top of anticlines in the pregrowth sequence (cf. Alonso, 1989).

Active Thrust-related Folding and Faulting

Chapters 8 and 9 both focus on active folding developed above thrust ramps. In both of these chapters, active thrust deformation is analyzed to validate the geometric models if the hanging wall folds.

Yue et al. (2011, Chapter 8) use 2-D seismic profiles and well-constrained surface geometries in pregrowth strata and deformed flights of fluvial terraces to develop plausible kinematic models through the active fold belt in western Taiwan. The authors describe two adjacent active thrust ramps in western Taiwan involving the same stratigraphic sequence and detachment; one is a large slip ramp (~14 km [8.7 mi]) with classic fault-bend fold geometries without limb rotation and the other is a low-slip ramp (1.7 km [1 mi]) with a hanging-wall limb rotation characteristic of shear fault-bend folding, suggesting a possible evolution in folding mechanism with increasing slip. The authors use the analysis of terrace folding, uplift, and tilting, together with the coseismic displacements in the 1999 Chi-Chi earthquake to validate these end-member kinematic models for thrust evolution.

Chapter 9 by Rivero and Shaw (2011) examines the thrust-related fold systems developed in the California borderlands, offshore southwest California, which has been considered a classic transpressional province. The authors relate the geometries of folds seen in seismic data to active earthquake faulting and active thrust systems associated with shortening and basin inversion in this complex contractional and strike-slip region. They propose that structural wedging, shear fault-bend folding, and fault-propagation folding are the most appropriate models to describe the evolution of these fold systems.

Basement-involved Thrust Systems

Wang et al. (2011, Chapter 10) integrated surface and subsurface data to produce a series of balanced geoseismic sections across the Kuqa fold belt, southern Tianshan ranges (on the northern edge of the Tarim Basin), western China. Here, the foreland basin deformation is linked to steep basement-involved, thrust uplifts of the main Tianshan ranges. In the foreland basin, both shear fault-bend folds (Suppe et al., 2004) and detachment fold systems were recognized. The frontal fold, the Yaken anticline, is active, deforming alluvial terraces and is interpreted to be an early stage in the formation of a detachment fold. Retrodeformed sections show how this complex, basement-involved fold and thrust belt developed and how active surface structures may be linked to thrust faulting at depth. This contribution is a significant new description of this important hydrocarbon-bearing fold and thrust belt.

Chapter 11 by Kraemer et al. (2011) analyzes the structural evolution of the Andean fold and thrust belt between 35°S and 36°S in western Argentina. Here, the Miocene–Pliocene deformation involves both basement thrusts as well as salt detachments in the cover strata. Syncontractional depocenters were bounded by active structures. Using a critical Coulomb wedge model, the authors explain the reactivation and uplift of hinterland structures during supercritical wedge times and enhanced deposition of synorogenic clastics during subcritical wedge times when reduced hinterland uplift was observed. This evolution is similar to that described in the analog models of Wu and McClay (2011, Chapter 14).

Mount et al. (2011) (Chapter 12) present a detailed analysis of wedge thrust systems involving basement in the Hanna Basin, Wyoming, western United States. Using long-offset seismic data, they describe two forms of wedge models where displacement on a deeper fault is transferred up section onto an oppositely dipping shallow fault. In the Hanna Basin example shown in this chapter, both basement-detached and basement-involved wedge structures are developed. Such indentor wedge structures are commonly seen at uplifted basin margins and at the termination of fold-thrust belts.

Quantitative Three-dimensional Analysis

Mencos et al. (2011) in Chapter 13 show how detailed field mapping combined with full 3-D construction of structural surfaces was essential in developing accurate 3-D geological and geometric models of growth-thrust-related detachment folds in the central Spanish Pyrenees. The authors incorporate surface geological data, digital elevation models, and orthophotos as well as seismic and well data to build a constrained 3-D geological model of a complex inversion-related anticline in the Bóixols thrust system of the central Spanish Pyrenees.

Scaled Analog Modeling of Thrust-related Fold Systems

Scaled physical laboratory models have been used extensively to illuminate the diverse issues in the kinematic evolution of fold and thrust belts. In Chapter 14, Wu and McClay (2011) describe the results of a detailed scaled analog modeling program designed to investigate the dynamic feedback and interactions of surface processes (synkinematic erosion and synkinematic sedimentation) on model fold and thrust belts as well as on individual folds within them. The analog models of fold and thrust belts form critically tapered Coulomb wedges (e.g., Davis et al., 1983). Within these wedges, synchronous thrusting on two or more active faults was focused toward the wedge front. In contrast, syntectonic erosion reduced the wedge taper, thereby promoting renewed thrusting at the rear of the wedge. Syntectonic sedimentation promoted focused deformation at the front of the wedge and changed the geometries of the thrust fault-related folds (e.g., Figure 7). These kinematic models show the complex slip history of fault-related folds in thrust belts and the episodic and cyclic nature of thrusting in these systems.

Deep-water Fold and Thrust Belts

In recent years, considerable exploration efforts have focused on deep-water fold belts where hanging-wall folds above either shale or salt detachments have been the main targets. Chapters 15 and 16 examine fold belt development offshore northeastern Brazil and in the offshore Nile Delta, respectively.

Chapter 15 by Zalán (2011) describes the 2-D and 3-D geometries of deep-water fold belts offshore northeastern Brazil. Here, the detachment is above ''overpressured'' shale systems. Complex imbricate thrust systems with hanging-wall fault-propagation folds are described and visualized in 3-D.

Chapter 16 by Krueger and Grant (2011) presents a detailed study of the fold systems in the offshore Niger Delta. These authors demonstrate that fault-propagation folds in the Niger Delta, once initiated, grew rapidly along strike reaching near-ultimate length early in the structural history and then subsequently amplified with the last stages of deformation focused in the central sections of the folds. This pattern of fold growth is attributed to the focusing of elevated pore-fluid pressures into the central section of the thrust-related fold system. The study has significant implications for fold growth mechanisms as well as for the timings of fold amplification and hence trapping of hydrocarbons in the toe-thrust systems of the Niger Delta.

SUMMARY

The chapters presented in this memoir cover some of the advances made in the study of thrust-related fold systems made over the past decade. Improved seismic imaging combined with theoretical, numerical, and analog modeling as well as detailed field studies has illuminated the challenges involved in integrating the well-established geometric and kinematic models of fault-related folding with mechanical models as well as being able to account for structures found in real-world examples of hydrocarbon-bearing structures. I hope that the readers of this memoir will find these new ideas and concepts relevant for the exploration and exploitation of hydrocarbon systems in fold and thrust belts worldwide.

ACKNOWLEDGMENTS

Ken McClay gratefully acknowledges the generous assistance of Jonny Wu, Jose de Vera, Hannah Rogers, and Nicola Scaselli with drafting and compiling the seismic images shown in this review. Alvar Braathen is thanked for use of the image in Figure 10b and Robert Burger for permission to use the photograph in Figure 10a. Stuart Hardy is thanked for the images of distinct element models of fault-related fold systems. Critical comments by John Suppe, John Shaw, Jose de Vera, and Stuart Hardy were greatly appreciated.

REFERENCES CITED

Ajakaiye, D. E., and A. W. Bally, 2002, Some structural styles on reflection profiles from offshore Niger Delta: AAPG Continuing Education Course Note 41, Course manual and atlas of structural styles from the Niger Delta, 107 p.

Allmendinger, R. W., 1998, Inverse and forward numerical modeling of trishear fault propagation folds: Tectonics, v. 17, no. 4, p. 640–656, doi:10.1029/98TC01907.

Alonso, J. L., 1989, Fold reactivation involving angular unconformable sequences: Theoretical analysis and natural examples from the Cantabrian zone (northwest Spain): Tectonophysics, v. 170, p. 57–77, doi:10.1016/0040-1951(89)90103-0.

Alonso, J. L., F. Colombo, and O. Riba, 2011, Folding mechanisms in a fault-propagation fold inferred from the analysis of unconformity angles: The Sant Llorenç growth structure (Pyrenees, Spain), *in* K. McClay, J. H. Shaw, and J. Suppe, eds., Thrust fault-related folding: AAPG Memoir 94, p. 137–151.

Atkinson, P. K., and W. K. Wallace, 2003, Competent unit thickness variation in detachment folds in the northeastern Brooks Range, Alaska: Geometric analysis and a conceptual model: Journal of Structural Geology, v. 25, no. 10, p. 1751–1771, doi:10.1016/S0191-8141(03)00003-8.

Beydoun, Z. R., M. W. Hughes Clarke, and R. Stoneley, 1992, Petroleum in the Zagros Basin: A Late Tertiary foreland basin overprinted onto the outer edge of a vast hydrocarbon-rich Paleozoic–Mesozoic passive-margin shelf, *in* R. W. Macqueen and D. A. Leckie, eds., Foreland basins and fold belts: AAPG Memoir 55, p. 309–339.

Bilotti, F., and J. H. Shaw, 2005, Deep-water Niger Delta fold and thrust belt modeled as a critical-taper wedge: The influence of elevated basal fluid pressure on structural styles: AAPG Bulletin, v. 89, no. 11, p. 1475–1491, doi:10.1306/06130505002.

Buxtorf, A., 1907, Zur Tektonik des Kettenjura: Beiricht der Versammlung des Oberrheinischen Geologischen Veireins, v. 40, p. 29–38.

Buxtorf, A., 1916, Prognosen und Befunde beim Hauensteinbasis–und Grechenberbtunnel und die Bedeutung der letzeren fur die Geologie des Jurabirges: Verhandlungen der naturforschenden Gesellschaft Basel, v. 27, p. 184–254.

Cooper, M. A., 2007, Structural style and hydrocarbon prospectivity in fold and thrust belts: A global review, *in* A. C. Ries, R. W. H. Butler, and R. H. Graham, eds., Deformation of the continental crust: The legacy of Mike Coward: Geological Society (London) Special Publication 272, p. 44–472.

Corredor, F., J. Shaw, and F. Bilotti, 2005a, Structural styles in the deep-water fold and thrust belts of the Niger Delta: AAPG Bulletin, v. 89, no. 6, p. 753–780, doi:10.1306/02170504074.

Corredor, F., J. Shaw, and J. Suppe, 2005b, Shear fault-bend folding, deep water Niger Delta, *in* J. Shaw, C. Connors, and J. Suppe, eds., Seismic interpretation of contractional fault-related folds: AAPG Studies in Geology 53, p. 87–92.

Cristallini, E. O., and R. W. Allmendinger, 2002, Backlimb trishear: A kinematic model for curved folds developed over angular fault bends: Journal of Structural Geology, v. 24, no. 2, p. 289–295.

Davis, D., J. Suppe, and F. A. Dahlen, 1983, Mechanics of fold-and-thrust-belts and accretionary wedges: Journal of Geophysical Research, v. 88, no. B2, p. 1153–1172, doi:10.1029/JB088iB02p01153.

Echavarria, L., R. Hernandez, R. Allmendinger, and J. Reynolds, 2003, Subandean thrust and fold belt of northwestern Argentina: Geometry and timing of the Andean evolution: AAPG Bulletin, v. 87, no. 6, p. 965–985.

Epard, J. L., and R. H. Groshong, 1995, Kinematic model of detachment folding including limb rotation, fixed hinges and layer-parallel strain: Tectonophysics, v. 247, no. 1–4, p. 85–103, doi:10.1016/0040-1951(94)00266-C.

Erslev, E. A., 1991, Trishear fault-propagation folding: Geology, v. 19, no. 6, p. 617–620, doi:10.1130/0091-7613(1991)019<0617:TFPF>2.3.CO;2.

Erslev, E. A., 1993, Thrusts, back-thrusts, and detachment of Laramide foreland arches, *in* C. J. Schmidt, R. Chase, and E. A. Erslev, eds., Laramide basement deformation in the Rocky Mountain foreland of the western United States: Geological Society of America Special Paper, v. 280, p. 339–358.

Erslev, E. A., and K. R. Mayborn, 1997, Multiple geometries and modes of fault-propagation folding in the Canadian thrust belt: Journal of Structural Geology, v. 19, no. 3–4, p. 321–335, doi:10.1016/S0191-8141(97)83027-1.

Gonzalez-Mieres, R., and J. Suppe, 2006, Relief and shortening in detachment folds: Journal of Structural Geology, v. 28, no. 10, p. 1785–1807, doi:10.1016/j.jsg.2006.07.001.

Gonzalez-Mieres, R., and J. Suppe, 2011, Shortening histories in active detachment folds based on area-of-relief methods, *in* K. McClay, J. H. Shaw, and J. Suppe, eds., Thrust fault-related folding: AAPG Memoir 94, p. 39–67.

Groshong Jr., R. H., and J. L. Epard, 1994, Role of strain in area-constant detachment folding: Journal of Structural Geology, v. 16, p. 613–618, doi:10.1016/0191-8141(94)90113-9.

Guzofski, C. A., J. P. Mueller, J. H. Shaw, P. Muron, D. A. Medwedeff, F. Bilotti, and C. Rivero, 2009, Insights into the mechanisms of fault-related folding provided by

volumetric structural restorations using spatially varying mechanical constraints: AAPG Bulletin, v. 93, no. 4, p. 479–502.

Hardy, S., and R. W. Allmendinger, 2011, Trishear: A review of kinematics, mechanics, and applications, *in* K. McClay, J. H. Shaw, and J. Suppe, eds., Thrust fault-related folding: AAPG Memoir 94, p. 95–119.

Hardy, S., and C. D. Connors, 2006, A velocity description of shear fault-bend folding: Journal of Structural Geology, v. 28, no. 3, p. 536–543, doi:10.1016/j.jsg.2005.12.015.

Hardy, S., and M. Ford, 1997, Numerical modeling of trishear fault propagation folding: Tectonics, v. 16, no. 5, p. 841–854, doi:10.1029/97TC01171.

Hardy, S., and K. McClay, 1999, Kinematic modelling of extensional forced folding: Journal of Structural Geology, v. 21, p. 695–702.

Hardy, S., and J. Poblet, 1994, Geometric and numerical model of progressive limb rotation in detachment folds: Geology, v. 22, no. 4, p. 371–374.

Hardy, S., J. Poblet, K. R. McClay, and D. Waltham, 1996, Mathematical modeling of growth strata associated with fault-related fold structures: Geological Society (London) Special Publication 99, p. 265–282.

He, D., J. Suppe, G. Yang, S. Guan, S. Huang, X. Shi, X. Wang, and C. Zhang, 2005, Guidebook for fieldtrip in south and north Tianshan foreland basin, Xinjiang Uygur Autonomous Region, China: International Conference on Theory and Application of Fault-Related Folding in Foreland Basins, Beijing, China, 78 p.

Homza, T. X., and W. K. Wallace, 1995, Geometric and kinematic models for detachment folds with fixed and variable detachment depths: Journal of Structural Geology, v. 17, no. 4, p. 575–588, doi:10.1016/0191-8141(94)00077-D.

Hubert-Ferrari, A., J. Suppe, R. Gonzalez-Mieres, and X. Wang, 2007, Mechanisms of active folding of the landscape (southern Tian Shan, China): Journal of Geophysical Research, v. 112, B03S09, p. 1–39, doi:10.1029/2006JB004362.

James, D. M. D., 1984, The geology and hydrocarbon resources of Negara Brunei Darussalam: Muzium Brunei, Bandar Seri Begawan, Brunei, p. 164.

Jamison, W. R., 1987, Geometric analysis of fold development in overthrust terranes: Journal of Structural Geology, v. 9, no. 2, p. 207–219.

Jordan, P., and T. Noack, 1992, Hanging wall geometry of overthrusts emanating from ductile decollements, *in* K. McClay, ed., Thrust tectonics: London, United Kingdom, Chapman & Hall, p. 311–318.

Kraemer, P., J. Silvestro, F. Achilli, and W. Brinkworth, 2011, Kinematics of a hybrid thick-thin-skinned fold and thrust belt recorded in Neogene syntectonic top-wedge basins, southern central Andes between 35° and 36°S, Malargüe, Argentina, *in* K. McClay, J. H. Shaw, and J. Suppe, eds., Thrust fault-related folding: AAPG Memoir 94, p. 245–270.

Krueger, S. W., and N. T. Grant, 2011, The growth history of toe thrusts of the Niger delta and the role of pore pressure, *in* K. McClay, J. H. Shaw, and J. Suppe, eds., Thrust fault-related folding: AAPG Memoir 94, p. 357–390.

Laubscher, H., 1965, Ein kinematisches modell der jurafaltung: Eclogae Geologicae Helvetiae, v. 58, p. 231–318.

Laubscher, H., 2008, The Grechenberg conundrum in the Swiss Jura: A case for the centenary of the thin-skin decollement nappe model (Buxtorf 1907): Swiss Journal of Geosciences, v. 101, p. 41–60, doi:10.1007/s00015-008-1248-2.

Maher, H. D., C. Craddock, and K. Maher, 1986, Kinematics of Tertiary structures in Upper Paleozoic and Mesozoic strata on Midterhuken, west Spitsbergen: Geological Society of America Bulletin, v. 97, p. 1411–1421.

Marrett, R., and P. A. Bentham, 1997, Geometric analysis of hybrid fault-propagation/detachment folds: Journal of Structural Geology, v. 19, p. 243–248, doi:10.1016/S0191-8141(96)00092-2.

McClay, K. R., 2004, Thrust tectonics and hydrocarbon systems: Introduction, *in* K. R. McClay, ed., Thrust tectonics and hydrocarbon systems: AAPG Memoir 82, p. ix–xx.

McQuarrie, N., 2004, Crustal-scale geometry of Zagros fold-thrust belt, Iran: Journal of Structural Geology, v. 26, no. 3, p. 519–535, doi:10.1016/j.jsg.2003.08.009.

Medwedeff, D., 1989, Growth fault-bend folding at southeast Lost Hills, San Joaquin Valley, California: AAPG Bulletin, v. 73, no. 1, p. 54–67.

Medwedeff, D. A., and J. Suppe, 1997, Multibend fault-bend folding: Journal of Structural Geology, v. 19, no. 3–4, p. 279–292, doi:10.1016/S0191-8141(97)83026-X.

Mencos, J., J. A. Muñoz, and S. Hardy, 2011, Three-dimensional geometry and forward numerical modeling of the Sant Corneli anticline (southern Pyrenees, Spain), *in* K. McClay, J. H. Shaw, and J. Suppe, eds., Thrust fault-related folding: AAPG Memoir 94, p. 283–300.

Mitra, S., 2002, Structrural models of faulted detachment folds: AAPG Bulletin, v. 86, no. 9, p. 1673–1694.

Mitra, S., 2003, A unified kinematic model for the evolution of detachment folds: Journal of Structural Geology, v. 25, no. 10, p. 1659–1673, doi:10.1016/S0191-8141(02)00198-0.

Mount, V. S., K. W. Martindale, T. W. Griffith, and J. O. D. Byrd, 2011, Basement-involved contractional wedge structural styles: Examples from the Hanna Basin, Wyoming, *in* K. McClay, J. H. Shaw, and J. Suppe, eds., Thrust fault-related folding: AAPG Memoir 94, p. 271–281.

Narr, W., and J. Suppe, 1994, Kinematics of basement-involved compressive structures: American Journal of Science, v. 294, no. 7, p. 802–860.

Poblet, J., and K. McClay, 1996, Geometry and kinematics of single-layer detachment folds: AAPG Bulletin, v. 80, no. 7, p. 1085–1109.

Poblet, J., K. McClay, F. Storti, and J. A. Munoz, 1997, Geometries of syntectonic sediments associated with single-layer detachment folds: Journal of Structural Geology, v. 19, no. 3–4, p. 369–381, doi:10.1016/S0191-8141(96)00113-7.

Poblet, J., M. Bulnes, K. McClay, and S. Hardy, 2004, Plots of crestal structural relief and fold area versus shortening—A graphical technique to unravel the kinematics of thrust-related folds, *in* K. R. McClay, ed., Thrust tectonics and hydrocarbon systems: AAPG Memoir 82, p. 372–399.

Rivero, C., and J. H. Shaw, 2011, Active folding and blind-thrust faulting induced by basin inversion processes, inner California borderlands, *in* K. McClay, J. H. Shaw, and J. H. Suppe, eds., Thrust fault-related folding: AAPG Memoir 94, p. 187–214.

Sandal, S. T., 1996, The geology and hydrocarbon resources of Negara Brunei Darussalam 1996 revision: Bandar Seri Begawan, Brunei Darussalam, Syabas, 243 p.

Shaw, J. H., C. D. Connors, and J. Suppe, 2005, Seismic interpretation of contractional fault-related folds: AAPG Studies in Geology 53, 156 p.

Sherkati, S., J. Letouzey, and D. Frizon de Lamotte, 2006, Central Zagros fold-thrust belt (Iran): New insights from seismic data, field observation, and sandbox modeling: Tectonics, v. 25, p. TC4007, doi:10.1029/2004TC001766.

Storti, F., and J. Poblet, 1997, Growth stratal architectures associated to decollement folds and fault-propagation folds. Inferences on fold kinematics: Tectonophysics, v. 282, no. 1–4, p. 353–373, doi:10.1016/S0040-1951(97)00230-8.

Suppe, J., 1983, Geometry and kinematics of fault-bend folding: American Journal of Science, v. 283, no. 7, p. 684–721.

Suppe, J., 1985, Principles of structural geology: New Jersey, Prentice Hall, 537 p.

Suppe, J., 2011, Mass balance and thrusting in detachment folds, *in* K. McClay, J. H. Shaw, and J. Suppe, eds., Thrust fault-related folding: AAPG Memoir 94, p. 21–37.

Suppe, J., and D. A. Medwedeff, 1990, Geometry and kinematics of fault-propagation folding: Eclogae Geologicae Helvetiae, v. 83, no. 3, p. 409–454.

Suppe, J., G. T. Chou, and S. C. Hook, 1992, Rates of folding and faulting determined from growth strata, *in* K. McClay, ed., Thrust tectonics: London, United Kingdom, Chapman & Hall, p. 105–121.

Suppe, J., F. Sabat, J. A. Muños, J. Poblet, E. Roca, and J. Verges, 1997, Bed-by-bed fold growth by kink-band migration: Sant Llorenç de Morunys, eastern Pyrenees: Journal of Structural Geology, v. 19, no. 3–4, p. 443–461, doi:10.1016/S0191-8141(96)00103-4.

Suppe, J., C. D. Connors, and Y. K. Zhang, 2004, Shear fault-bend folding, *in* K. McClay, ed., Thrust tectonics and hydrocarbon systems: AAPG Memoir 82, p. 303–323.

Tankard, A. J., R. Suarez-Soruco, and H. J. Welsink, 1995, Petroleum basins of South America: AAPG Memoir 62, 792 p.

Tavani, S., and F. Storti, 2011, Layer-parallel shortening temples associated with double-edge fault-propagation folding, *in* K. McClay, J. H. Shaw, and J. Suppe, eds., Thrust fault-related folding: AAPG Memoir 94, p. 121–135.

Vergés, J., M. G. H. Goodarzi, H. Emami, R. Karpuz, J. Efstathiou, and P. Gillespie, 2011, Multiple detachment folding in Pusht-e Kuh arc, Zagros: Role of mechanical stratigraphy, *in* K. McClay, J. H. Shaw, and J. Suppe, eds., Thrust fault-related folding: AAPG Memoir 94, p. 69–94.

Wang, X., J. Suppe, S. Guan, A. Hubert-Ferrari, R. Gonzalez-Mieres, and C. Jia, 2011, Cenozoic structure and tectonic evolution of the Kuqa fold belt, southern Tianshan, China, *in* K. McClay, J. H. Shaw, and J. Suppe, eds., Thrust fault-related folding: AAPG Memoir 94, p. 215–243.

Wu, J. E., and K. R. McClay, 2011, Two-dimensional analog modeling of fold and thrust belts: Dynamic interactions with syncontractional sedimentation and erosion, *in* K. McClay, J. H. Shaw, and J. Suppe, eds., Thrust fault-related folding: AAPG Memoir 94, p. 301–333.

Yue, L.-F., J. Suppe, and J.-H. Hung, 2011, Two contrasting kinematic styles of active folding above thrust ramps, western Taiwan, *in* K. McClay, J. H. Shaw, and J. Suppe, eds., Thrust fault-related folding: AAPG Memoir 94, p. 153–186.

Zalán, P. V., 2011, Fault-related folding in the deep waters of the equatorial margin of Brazil, *in* K. McClay, J. H. Shaw, and J. Suppe, eds., Thrust fault-related folding: AAPG Memoir 94, p. 335–355.

Zehnder, A. T., and R. W. Allmendinger, 2000, Velocity field for the trishear model: Journal of Structural Geology, v. 22, no. 8, p. 1009–1014, doi:10.1016/S0191-8141(00)00037-7.